Carey-Smith, B. E., Warr, P. A., Beach, M. A., & Nesimoglu, T. (2005). Wide tuning-range planar filters using lumped-distributed coupled resonators. IEEE Transactions on Microwave Theory and Techniques, 53(2), 777 - 785. [Issue 2]. 10.1109/TMTT.2004.841221

Wide Tuning-Range Planar Filters Using Lumped-Distributed Coupled Resonators

Bruce E. Carey-Smith, Paul A. Warr, Mark A. Beach, *Associate Member, IEEE*, and Tayfun Nesimoglu

***Abstract*—This paper describes a discretely tunable filter topology based on lumped-distributed coupled transmission lines, particularly suitable for microelectromechanical systems switching devices. This topology is capable of simultaneous wide-band center frequency and bandwidth tuning, limited only by the electrical size of the transmission lines and the placement density of the switching devices. Low fractional bandwidths can be achieved without the need for large coupled-line spacings due to the antiphase relationship of the lumped capacitive and distributed electromagnetic coupling coefficients. The positions of the additional poles of attenuation due to the lumped capacitive coupling can be selected either above or below band leading to the choice of a narrow bandwidth design having good high-side performance or a design with compromised upper stopband performance, but with no bandwidth tuning limitations. The interaction between a pair of lumped-distributed coupled transmission lines is analyzed and the resulting model is used to develop a filter synthesis procedure. The synthesis procedure and filter performance are validated through theoretical and experimental comparisons using a filter with low-side attenuation poles.**

***Index Terms*—Discrete tuned, filter synthesis, lumped-distributed coupled transmission lines, microelectromechanical systems (MEMS), microwave bandpass filters, tunable filters.**

I. Introduction

INVESTIGATION into the implementation of software reconfigurable radio has highlighted the importance of flexible receiver front-end filtering [1]. In order to take advantage of a diverse range of wireless channels and standards, a wide range of frequencies and bandwidths should be selectable. A single reconfigurable filter capable of operating over the complete range is likely to offer significant savings in terms of size and system complexity.

The continuing maturation of RF microelectromechanical systems (RF MEMS) has led to the possibility of wide-range tunable filters with low current consumption, low distortion, and potentially low cost. These devices have been used as alternative tuning elements in filters traditionally tuned using varactor and p-i-n diodes, but they have also prompted the design of new tunable filter topologies.

The use of RF MEMS as the tuning elements in lumped-element filters has been demonstrated [2]–[5]. Due to the lack of high-Q MEMS-tunable inductors, the majority of these designs use lumped air-core inductors, the tuning being done using MEMS capacitors. Octave center frequency and 6 : 1 bandwidth tuning ranges have been reported [5].

Manuscript received April 23, 2004; revised July 30, 2004. This work was supported in part by the European Union under the Information Society Technologies Project IST-2001-34091.

The authors are with the Centre for Communications Research, University of Bristol, Bristol BS8 1UB, U.K. (e-mail: carey-smith@bristol.ac.uk).

Digital Object Identifier 10.1109/TMTT.2004.841221

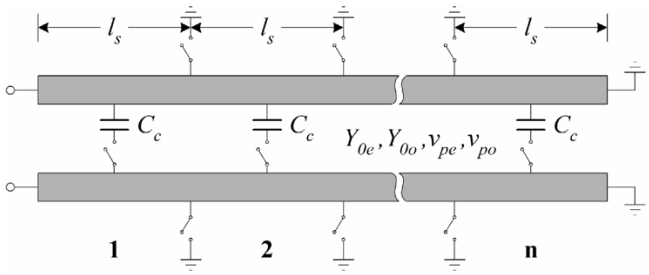

Fig. 1. Lumped-distributed quarter-wave coupled resonators. From [10].

RF MEMS have also been used to tune distributed filters. The center frequency of this class of filter can be altered by direct physical transmission-line length adjustment [6] or by the indirect capacitive loading of the resonant transmission-line elements [7], [8]. Bandwidth tuning is less common in planar filters due to the difficulties of adjusting the inter-resonator coupling. Tunable lumped-element coupling tends to alter the characteristics of the resonators, obligating the additional control of their resonant frequency [9]. Center frequency and bandwidth tuning by independent control of attenuation poles has been successfully demonstrated, however, the frequency dependence of the quarter-wavelength impedance inverters placed a severe limitation on the center-frequency tuning range of the design [8].

This paper investigates a wide center-frequency and bandwidth tuning range filter utilizing lumped-distributed coupled transmission-line resonators. The coupled resonator structures employed are particularly suitable for use with RF MEMS contact and capacitive switches. They allow wide range tuning of both the resonant frequency and coupling coefficient, limited only by the electrical size of transmission lines and the placement density of the RF MEMS devices. Futhermore, the use of multiple distributed tuning elements results in a flexible structure where the resonator unloaded Q remains independent of the tuning mechanism [10]. In order to achieve this, a modified combline topology is adopted, consisting of pairs of grounded quarter-wavelength coupled resonators whose input and output terminals are at the same end. The structure becomes tunable by incorporating switchable coupling capacitors and switchable ground connections along the length of the resonator lines (Fig. 1). The advantages of this topology are threefold: firstly, only a single grounding switch is in-circuit regardless of the selected length, therefore, the impact of resistive switch losses on the resonator Q remains constant. Secondly, it retains a constant overlap region and coupling factor regardless of the coupled-line length. Finally, because the electromagnetic (EM)

coupling between the transmission lines is antiphase to the lumped capacitive coupling, very low coupling coefficients can be obtained regardless of coupled-line spacing.

Using mathematical models developed in Section II, the coupling coefficient and transmission characteristics of the structure can be analyzed. The lumped-distributed capacitive coupling introduces an additional attenuation pole and it is shown that the antiphase relationship between the modes of coupling allows this pole to be placed either above or below the primary passband.

A filter synthesis technique based on these models is introduced in Section III. Using this technique, the initial filter parameters can be derived from standard filter prototype values.

The tuning performance of the filter is presented visually and discussed in Section IV. The theoretical filter performance and synthesis procedure are then verified through the design and measured results of a third-order lumped-distributed coupled-line filter realized in coplanar waveguide.

II. Lumped-Distributed Coupled Lines

A pair of lumped-distributed coupled lines is shown in Fig. 1 having a per-unit-length coupling capacitance

$$C_{cm} = \frac{C_c}{l_s} \tag{1}$$

and a coupled region length

$$l = n \cdot l_s. \tag{2}$$

A. Mathematical Circuit Model

A mathematical model of the lumped-distributed coupled-line section can be derived in several ways. A model that describes the true periodic nature of the lumped-distributed structure can be derived by using a combination of periodic and even- and odd-mode circuit analyses. However, it is also possible to model the circuit as purely distributed, leading to greatly simplified equations. A lumped-distributed structure exhibits its first stopband when its guided wavelength approaches the periodic spacing of the lumped components. At well below this stopband, the structure can be accurately approximated as purely distributed. This is the approach taken here.

A pair of coupled lines can be described in terms of their even- and odd-mode characteristic admittances (Y_{0e}, Y_{0o}) and phase velocities (v_{pe}, v_{po}). In the quasi-static case, these even- and odd-mode parameters can be represented in terms of equivalent lumped per-unit-length inductances and capacitances, as shown in Fig. 2 [11]. The relationships are

$$\begin{aligned} Y_{0e} &= \sqrt{\frac{C_a}{L_a + L_m}} \\ Y_{0o} &= \sqrt{\frac{C_a + 2C_m}{L_a - L_m}} \end{aligned} \tag{3}$$

$$\begin{aligned} v_{pe} &= \sqrt{C_a(L_a + L_m)} \\ v_{po} &= \sqrt{(C_a + 2C_m)(L_a - L_m)} \end{aligned} \tag{4}$$

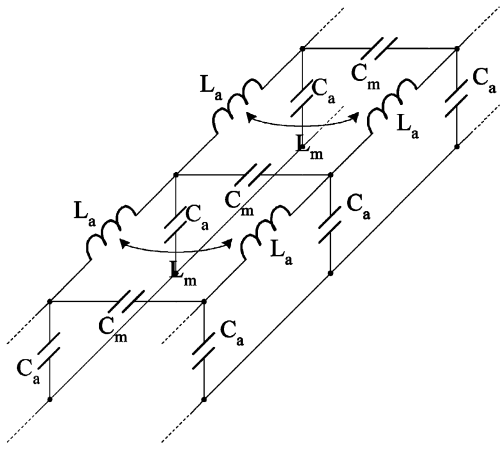

Fig. 2. Lumped equivalent circuit of coupled transmission lines.

where C_a and L_a are the self-capacitance and inductance of one of the lines and C_m and L_m are the mutual capacitance and inductance between the coupled lines. Equations (3) and (4) can be rearranged to find the value of the equivalent lumped-circuit elements

$$\begin{aligned} C_a &= \frac{Y_{0e}}{v_{pe}} \\ C_m &= \frac{1}{2}\left[\frac{Y_{0o}}{v_{po}} - \frac{Y_{0e}}{v_{pe}}\right] \end{aligned} \tag{5}$$

$$\begin{aligned} L_a &= \frac{1}{2}\left[\frac{Z_{0e}}{v_{pe}} + \frac{Z_{0o}}{v_{po}}\right] \\ L_m &= \frac{1}{2}\left[\frac{Z_{0e}}{v_{pe}} - \frac{Z_{0o}}{v_{po}}\right]. \end{aligned} \tag{6}$$

Additional inter-line coupling capacitance C_{cm} will have no effect on the parameters C_a, L_a, and L_m and, as a consequence, the even-mode parameters Y_{0e} and v_{pe} will remain unchanged. However, the odd-mode parameters will be affected and, by making use of (3)–(6) the new values Y'_{0o} and v'_{po} can be expressed in terms of the original odd-mode parameters and the additional per-unit-length coupling capacitance C_{cm}. The result is

$$v'_{po} = v_{po}\sqrt{\frac{Y_{0o}}{Y_{0o} - 2v_{po}C_{cm}}} \tag{7}$$

and

$$Y'_{0o} = \sqrt{Y_{0o}(Y_{0o} - 2v_{po}C_{cm})}. \tag{8}$$

The admittance parameters of a symmetrical two-port network are related to the even- and odd-mode input admittances by the following two expressions:

$$y_{11} = \frac{y_{11e} + y_{11o}}{2} \text{ and } y_{12} = \frac{y_{11e} - y_{11o}}{2}. \tag{9}$$

Since the one-port even- and odd-mode input admittances of the lumped-distributed coupled-line model both have the form

$$y_{11e,o} = -jY_{0e,o}\cot\theta_{e,o} \tag{10}$$

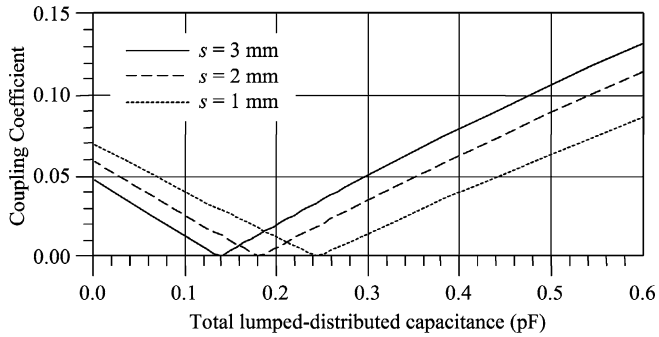

Fig. 3. Coupling coefficient of lumped-distributed coupled lines indicating that the capacitive coupling is in antiphase to the EM coupling.

where $\theta_{e,o}$ are the even- or odd-mode coupled-line phase lengths, the two-port admittance parameters can be written as

$$y_{11} = -\frac{j}{2}\left(Y_{0e}\cot\left(\frac{\omega\cdot l}{v_{pe}}\right) + Y'_{0o}\cot\left(\frac{\omega\cdot l}{v'_{po}}\right)\right) \tag{11}$$

and

$$y_{12} = -\frac{j}{2}\left(Y_{0e}\cot\left(\frac{\omega\cdot l}{v_{pe}}\right) - Y'_{0o}\cot\left(\frac{\omega\cdot l}{v'_{po}}\right)\right). \tag{12}$$

where ω is the angular velocity and l is the coupled-line length.

B. Coupling Coefficient Analysis

Using the formulation developed in [12], the coupling coefficient of the lumped-distributed coupled-line structure can be found from its simulated frequency response. Typical results are shown in Fig. 3 where the coupling coefficient for a pair of coupled microstrip lines is plotted against the total lumped capacitance for various values of coupled-line spacing s. The change in gradient of the coupling coefficient, from negative to positive, is indicative that, for this coupled-line configuration, the distributed EM coupling is primarily magnetic in nature and is in antiphase to the direct capacitive coupling. The result is that, at low values of lumped coupling capacitance, the coupling coefficient is actually reduced, allowing the coupling coefficient and, therefore, the filter bandwidth, to be controlled down to a very low value without the need for large coupled-line spacings.

The electric and magnetic coupling coefficients are the ratio of coupled-to-stored electric and magnetic energy. In the quasi-static case, they can be derived from the capacitance and inductance elements of the lumped equivalent circuit. Summing the two yields the total mixed coupling, which, for this configuration, takes the form

$$k = \left|\frac{C_m + C_{cm}}{C_a + C_m + C_{cm}} - \frac{L_m}{L_a}\right|. \tag{13}$$

C. Transmission Characteristics

Using two-port circuit analysis, the ratio of input-to-output voltage or voltage attenuation function $A(j\omega)$ for a pair of same-end-shorted coupled lines terminated in a source and load admittance Y_g can be found from (11) and (12) as

$$A(j\omega) = \frac{(jY_{0o}\cot\theta_o - Y_g)(Y_g - jY_{0e}\cot\theta_e)}{j2Y_g(Y_{0e}\cot\theta_e - Y_{0o}\cot\theta_o)}. \tag{14}$$

Poles of attenuation occur when the denominator of (14) is equal to zero. This condition is satisfied when $Y_{0o}\cot\theta_o = Y_{0e}\cot\theta_e$. For purely distributed same-end-grounded coupled lines in a nonhomogenous medium, the condition for a pole of attenuation is met only at dc. Complete transmission corresponds to zeros in the numerator, which occur when either $jY_{0o}\cot\theta_o$ or $jY_{0e}\cot\theta_e$ equal Y_g. This indicates that the primary passband is centered between the even- and odd-mode quarter-wavelength frequencies, its width being dependent on the ratio of $|Y_g|$ to Y_{0e} and Y_{0o}. Further passbands occur at all odd harmonic frequencies.

The lumped capacitance C_{cm} introduces an additional attenuation pole. At low values of capacitance, where the coupling is still primarily magnetic, the pole appears above the primary passband. As the capacitance is increased, the pole frequency reduces until the pole and zero frequencies coincide and the primary passband disappears. The value of capacitance at which this occurs can be found by substituting (5) and (6) into (13) and setting $k = 0$. This value corresponds to the point of gradient change in Fig. 3 and is given by

$$C_{cm0} = \frac{Y_{0e}\left(v_{po}^2 - v_{pe}^2\right)}{2v_{po}v_{pe}^2}. \tag{15}$$

When the lumped capacitance is larger than this value, the pole appears below the primary passband. Accordingly, two regions of variable coupling coefficient can be defined above and below C_{cm0}. Using adjustable lumped capacitance in the lower region results in a bandwidth tunable filter with better high-side rejection. However, the maximum achievable bandwidth in this case occurs when the lumped capacitance is set to zero and will be dictated by the EM coupling that can be achieved. The maximum amount of EM coupling that can be obtained from a pair of same-end-grounded coupled lines is limited by the degree to which the structure supports unequal odd- and even-mode wave velocities. In practice, this will limit the use of the high-side pole variant to narrow-band filters.

However, using adjustable coupling capacitance in the second region (above C_{cm0}), although giving compromised upper stopband performance, does lead to a design where the maximum bandwidth is limited only by the capacitance value.

III. Synthesis

A technique for deriving filter design equations is described in [13]. It is based on Cohn's direct-coupled filter synthesis technique [14]; however, rather than relying on the derivation of expressions for the inverter and resonator slope parameters, it simply compares the admittance and phase of sections of the filter to be designed with those of a generic inverter-coupled filter, forcing the two to correspond at specific points in the filter passband. The interior sections of the filters are described and compared in terms of their image parameters, while the end sections are compared by defining an admittance seen looking

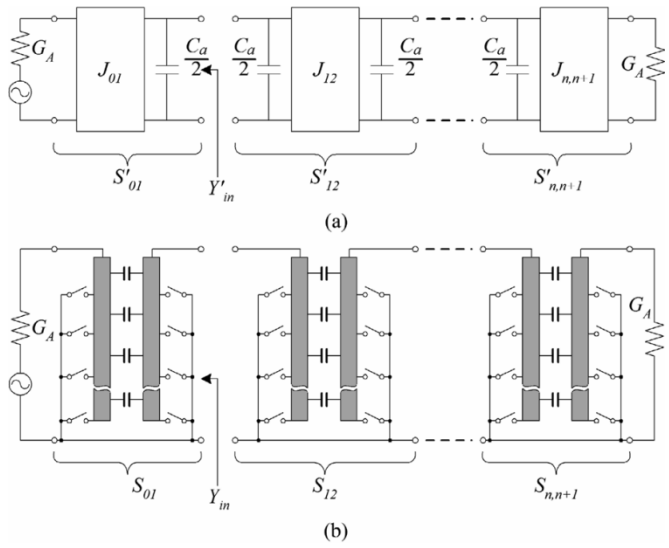

Fig. 4. (a) Generic inverter-coupled filter circuit and (b) lumped-distributed coupled-resonator filter circuit divided into symmetrical sections.

through them toward the source. This method is useful for filter circuits where the inverter and resonator functions cannot be mapped directly to those of the generic inverter coupled filter.

The circuit divisions of the generic inverter-coupled filter are shown in Fig. 4(a), where the sections are indicated by labels S'_{01}–$S'_{n,n+1}$. The circuit is a modified form of the standard filter prototype circuit, which uses only one kind of reactive element along with admittance inverters J_{01} to $J_{n,n+1}$. The admittance inverters are assumed to be ideal and frequency independent. The image admittance $Y'_{k,k+1}$ and phase $\beta'_{k,k+1}$ for the interior sections of the modified prototype circuit (S'_{12}–$S'_{n-1,n}$) are given by

$$Y'_{k,k+1} = hG_A\sqrt{\frac{4-\omega'}{4g_kg_{k+1}}} \tag{16}$$

$$\cos\beta'_{k,k+1} = \frac{\omega'\sqrt{g_kg_{k+1}}}{2} \tag{17}$$

under the condition that the capacitors $C_a = hG_A$, where h is an arbitrary admittance scaling factor, G_A is the terminating conductance, g_k and g_{k+1} are the low-pass filter prototype element values, and ω' is the angular frequency of the low-pass prototype filter having a cutoff frequency $\omega' = 1$ rad. The admittance $Y'_{\rm in}$, needed to relate the end sections of the filters, is defined by looking at the source through the end section of the modified prototype circuit, as shown in Fig. 4(a). Given that $C_a = hG_A$, it is easily seen that

$$Y'_{\rm in} = \frac{J_{01}^2}{G_A} + j\omega'\frac{hG_A}{2}. \tag{18}$$

The division of the lumped-distributed coupled-resonator filter into symmetrical sections is shown in Fig. 4(b). Each of the sections consists of a single pair of coupled resonators. The image admittance $Y_{k,k+1}$ and phase $\beta_{k,k+1}$ can be found directly from the two-port y-parameter expressions derived in Section II by using the following relations:

$$Y_{k,k+1} = \sqrt{y_{11}^2 - y_{12}^2} \tag{19}$$

$$\cos\beta_{k,k+1} = \frac{y_{11}}{y_{12}}. \tag{20}$$

The admittance $Y_{\rm in}$ of the end sections can be obtained by using the y-parameter Π-network equivalent circuit

$$Y_{\rm in} = \frac{y_{11}^2 + y_{11}G_A + y_{12}^2}{y_{11} + G_A}. \tag{21}$$

A. Conditions of Correspondence for Interior Sections

When relating the lumped-distributed coupled resonator filter to the modified prototype, the use of the parameter correspondences from [13] leads to an error in the center frequency and bandwidth of the resultant filter. This error is caused by the asymmetric passband response of the lumped-distributed coupled-line circuit and is proportional to the value of capacitive coupling. The correspondence can be improved through the use of a frequency-mapping function derived by equating the image phase of the two circuits (17) and (20) as follows:

$$\frac{Y_{0e}\cot\left(\frac{\omega_s\cdot l}{v_{pe}}\right) + Y'_{0o}\cot\left(\frac{\omega_s\cdot l}{v'_{po}}\right)}{Y_{0e}\cot\left(\frac{\omega_s\cdot l}{v_{pe}}\right) - Y'_{0o}\cot\left(\frac{\omega_s\cdot l}{v'_{po}}\right)} = \frac{\omega'\sqrt{g_kg_{k+1}}}{2} \tag{22}$$

where ω_s is the new scaled frequency variable. The interior sections S'_{12}–$S'_{n-1,n}$ of the modified prototype are then related to the interior sections S_{12}–$S_{n-1,n}$ of the coupled-line circuit by forcing the following correspondences:

$$\beta_{k,k+1}|_{\omega=\omega_1} = \beta'_{k,k+1}|_{\omega'=1} \tag{23}$$

$$\beta_{k,k+1}|_{\omega=\omega_2} = \beta'_{k,k+1}|_{\omega'=-1} \tag{24}$$

$$Y_{k,k+1}|_{\omega=\omega_{s0}} = Y'_{k,k+1}|_{\omega'=0}. \tag{25}$$

where ω_{s0} is the value of the scaled frequency variable ω_s from (22) corresponding to $\omega' = 0$, and ω_1 and ω_2 are the lower and upper band edge frequencies related to the band center frequency ω_0 and fractional bandwidth W by

$$\omega_1 = \omega_0\left(1 - \frac{W}{2}\right) \text{ and } \omega_2 = \omega_0\left(1 + \frac{W}{2}\right). \tag{26}$$

The effect of these correspondences is to force the correct phase conditions at the band edges of the coupled-line section, while at the same time, ensuring that the image admittance is the correct value at the electrical band center ω_{s0} (where $\beta_{k,k+1} = 90°$). Solving the three resulting equations simultaneously for given values of $g_k, g_{k+1}\,\omega_0, W, Z_{0e}, Z_{0o}, v_{pe}$, and v_{po} yields a solution in terms of the coupled-line length l, coupling capacitance C_{cm}, and the admittance scaling factor h for each interior section. The admittance scaling factor must be held constant throughout the filter. When the number of interior sections exceeds two, this no longer occurs coincidentally, and the interior sections must be solved in an iterative manner; firstly,

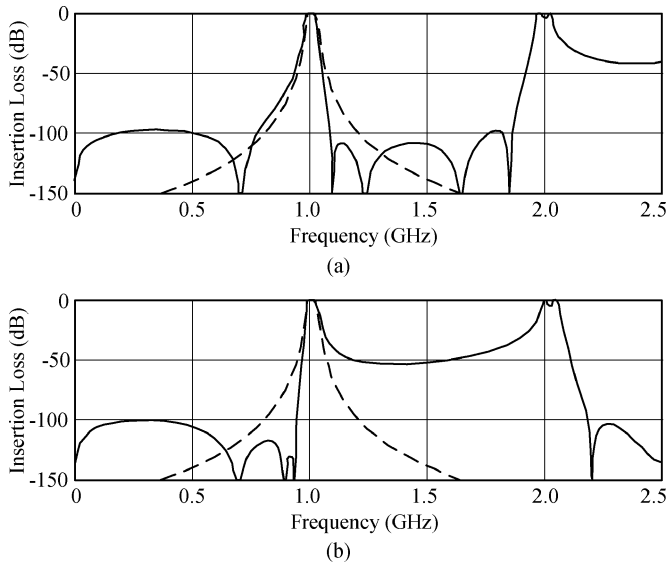

Fig. 5. Response of an ideal fifth-order synthesized lumped-distributed coupled-resonator filter (solid line) compared to the prototype filter response (broken line). Additional poles of attenuation: (a) above and (b) below the passband.

to find the required value of h to give reasonable admittance levels and, secondly, for the coupled-line parameter values for each of the interior sections.

B. Conditions of Correspondence for End Sections

The end sections S'_{01} and $S'_{n,n+1}$ of the modified prototype are related to their corresponding coupled-line end sections S_{01}–$S_{n,n+1}$ by forcing the following correspondences:

$$\beta_{k,k+1}|_{\omega=\omega_{s0}} = \frac{\pi}{2} \tag{27}$$

$$\mathrm{Re}\,(Y_{\mathrm{in}}|_{\omega=\omega_{s0}}) = \mathrm{Re}\,(Y'_{\mathrm{in}}|_{\omega'=0}) \tag{28}$$

where ω_{s0} is the electrical band center derived from the interior sections. The first correspondence ensures that the electrical band center for the end sections aligns with that of the interior sections, while the second correspondence forces the correct admittance transformation level into and out of the filter. As with the interior sections, the two resulting equations can be solved simultaneously using numerical methods and a solution found in terms of the coupled-line length l and coupling capacitance C_{cm} for given values of g_k, g_{k+1} ω_0, W, Z_{0e}, Z_{0o}, v_{pe}, v_{po}, and h.

Once the design values for the individual sections have been found, the complete filter can be constructed by connecting the near-side resonators of adjacent sections to form a series of half-wavelength resonators coupled to each other along half their length. The filter differs from a quarter-wave combline topology in this respect, but the difference is necessary in order to accommodate the grounded MEMS switches. Unfortunately, the resulting structure supports passbands at all harmonic frequencies. This can be observed in Fig. 5, where the responses of an ideal fifth-order lumped-distributed coupled resonator filter are plotted with the poles of attenuation placed above and below the passband, respectively.

Fig. 5 also illustrates the improvement in upper stopband attenuation using the high-side attenuation pole.

IV. Tuning Analysis

Using the equations developed in Section III, a filter can be designed from a number of lumped-distributed coupled-line sections. Solving these equations results in specific values of coupling capacitance and line length for a given filter center frequency and fractional bandwidth. Once these initial design values have been selected, the filter is tuned by the discrete switching of ground connections and coupling capacitors. Since the tuning is not continuous, only certain values of center frequency and bandwidth can be obtained. Furthermore, the relationships between coupling capacitance, resonator length, fractional bandwidth, and center frequency are not linear.

From (3) and (4), it is clear that the coupling capacitance acts to reactively load the transmission lines, altering their odd-mode characteristic impedance and phase velocity. As the coupling capacitance is tuned, the effective phase velocity and, consequently, the resonant frequency of the transmission lines is altered. However, this change in phase velocity is not consistent throughout the filter. To achieve the impedance transformation required in practical transmission-line filters, the coupling capacitors of the filter end sections must be significantly larger than those of the interior sections. Changing the bandwidth involves scaling the inter-resonator coupling throughout the filter and the disproportionate size of the end section coupling capacitors means that their scaling has a greater effect on the phase velocity. This leads to a misalignment of end and interior section resonant frequencies, ultimately distorting the filter shape. Continuously variable resonator lengths could compensate for this by incremental adjustment; however, this is not possible in the discrete design. The result is that a good filter shape is only available at certain tuning points.

In order to gain an appreciation of this effect, it is helpful to plot the points where good filter shape can be achieved on the two-dimensional tuning surface of the lumped-distributed coupled resonator filter; fractional bandwidth versus center frequency. To do so, a measure of a particular tuning point's deviation from the desired filter characteristics is required. One way of expressing this deviation is to determine the line length and coupling capacitance of each filter section required for a particular fractional bandwidth and center frequency. The deviations of each of these length and capacitance values from the available discrete values can then be combined to give an overall error value. Plotting this error value on a contour plot versus center frequency and bandwidth gives a visual representation of the tuning performance of a particular filter. As an example, the error contour plot for the experimental filter to be introduced in Section V is shown in Fig. 6. The experimental filter has four lumped-distributed coupled-line sections and eight length (l_s) and capacitance (C_c) parameters. Due to the filter symmetry, only four of these are needed to find the overall error. This error value will vary between zero, for a perfect filter shape, and two, for maximum error. In the latter case, every length and capacitance parameter is exactly midway between discrete tuning points.

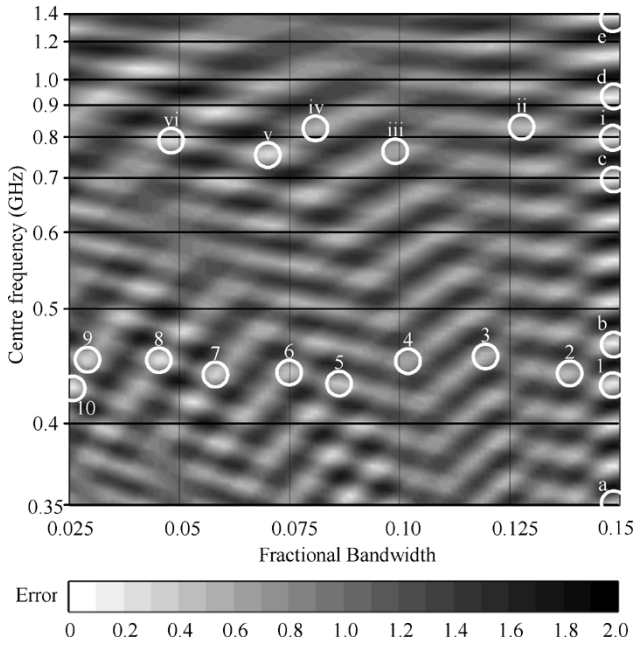

Fig. 6. Contour plot of filter shape error on the two-dimensional tuning space; fractional bandwidth and center frequency. Points circled on the plot are discussed in Section V.

The plot shows a series of good tuning points at the initial design fractional bandwidth (which, in this case, is equal to 0.15), uniformly spaced at frequencies corresponding to the discrete length tuning points. This occurs because, in this design, all of the filter sections have the same number of tunable length segments, resulting in the synchronous tuning of their electrical lengths.

For different values of fractional bandwidth, the relationship becomes more complex. As alluded to earlier, this is caused by the changes in per-unit-length coupling capacitance. The result is that the points on the tuning surface, which yield good filter performance, follow nonequispaced lines, which diverge as the center frequency increases. The tuning surface plot provides a useful aid in visualizing these relationships and in selecting the appropriate tuning points for desired filter characteristics.

V. Experimental Results

To verify the theoretical analysis of Section IV and to test the lumped-distributed coupled-line filter's tuning capabilities, a third-order filter with 16 tunable segments was designed and fabricated based on a Butterworth prototype. A coplanar-waveguide medium was used, as it allows well-defined and easily adjustable ground connections for the resonators. The intention was to provide electronically controlled center-frequency and bandwidth tuning through the use of MEMS switches and MEMS bi-stable capacitors; however, for prototyping purposes, the transmission-line lengths and lumped coupling capacitance were adjusted manually through the use of removable printed links to ground, and surface-mount 0603-size capacitors. The filter was designed to operate in the region above C_{cm0} (refer to Section II-C) having a maximum fractional bandwidth of 15% with all coupling capacitors in circuit. The design center-frequency tuning range of the filter was from 350 MHz (16 segments) to 1.4 GHz (four segments). A low-loss microwave laminate was used ($h = 1.52\,\text{mm}, \varepsilon_r = 3.05, \tan\delta = 0.003$). Various critical dimensions of the coupled lines of the filter were preselected based on the parameters of this laminate, and are given in Table I.

TABLE I
Preselected Coupled-Line Dimensions

Parameter		Value	Units
w	Transmission-line width	1.3	*mm*
s	Coupled-line spacing	3.0	*mm*
g	Co-planar ground spacing	1.5	*mm*
d	Min. adjacent coupled line pair spacing	10	*mm*
Z_{0e}	Even-mode characteristic impedance	90.218	Ω
Z_{0o}	Odd-mode characteristic impedance	79.950	Ω
v_{pe}	Even-mode phase velocity	1.96×10^8	*m/s*
v_{po}	Odd-mode phase velocity	2.04×10^8	*m/s*

TABLE II
Unit Length and Coupling Capacitance for Experimental Filter

	l_s	C_c
End sections: S_{01}	4.920 mm	0.601 pF
Interior sections: S_{12}	7.398 mm	0.195 pF

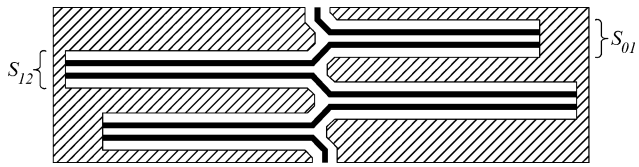

Fig. 7. Diagram of experimental lumped-distributed coupled-line line filter.

A full-wave EM simulation was used to extract the even- and odd-mode characteristic impedances and phase velocities of a pair of coplanar-waveguide coupled lines with these critical dimensions and a lower ground plane. These are also listed in Table I. Using these coupled-line parameters and the appropriate prototype filter element values, the unit length l_s and coupling capacitance C_c for both the interior and end sections were derived using the technique described in Section III. The resulting values are given in Table II.

A lumped-distributed coupled-line filter prototype was fabricated using standard lithography techniques. A drawing of the resultant filter layout is shown in Fig. 7; for clarity, the switchable coupling capacitors and ground connections are not shown. The filter measures approximately 44×240 mm.

A hybrid model for the lumped-distributed coupled-line filter was built up from analytical and full-wave EM simulations using Agilent Technologies ADS. To reduce the simulation time and allow for the inclusion of multiple lumped components, EM simulations were only carried out on smaller circuit segments and the resulting data was integrated into an analytical simulation in the form of S-parameter blocks. The periodic nature of the lumped-distributed coupled-line circuit meant it was well-suited to this hybrid approach. This EM and analytical hybrid model was used to simulate the response of

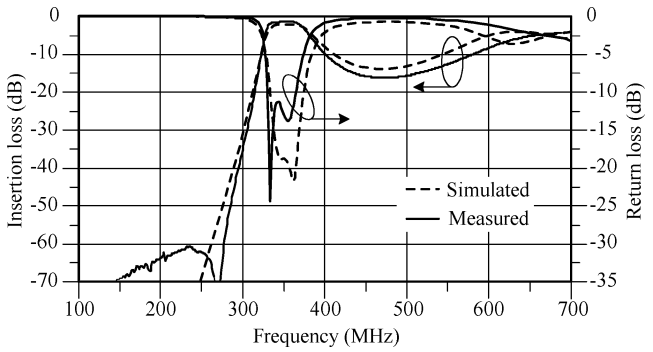

Fig. 8. Measured (solid line) and simulated (broken line) response for lumped-distributed coupled-line filter at the initial design frequency and bandwidth.

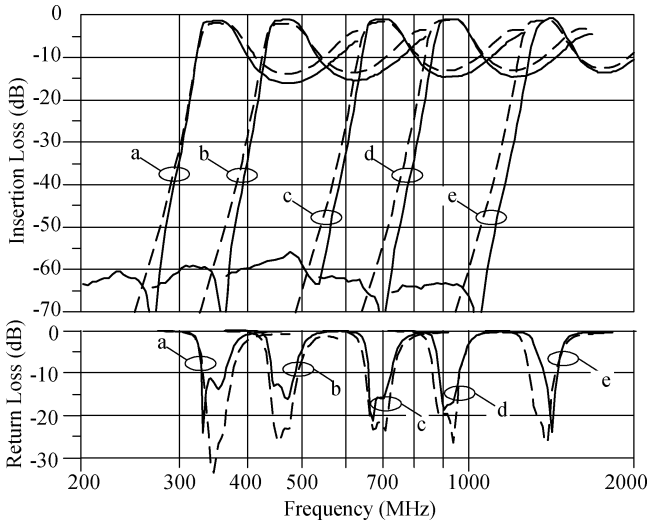

Fig. 9. Simulated (broken line) and measured (solid line) results for five of the 16 possible tuning states of the experimental lumped-distributed coupled-line filter. The indexing terms, a–e refer to Fig. 6. Data from [10].

the experimental filter. This is presented in Fig. 8 along with the measured results of the filter at the initial design frequency and bandwidth. For medium bandwidths and low filter order the upper stopband rejection is poor, however, the simulated response shows reasonable correlation with the measured results. The increase in frequency of the low-side attenuation pole has been shown to be caused by cross-coupling between nonadjacent resonators.

A. Center-Frequency Tuning

Although many different center-frequency tuning states are possible, the largest number having constant fractional bandwidth occur at the design value of 0.15, as discussed in Section IV. These tuning states can be obtained by switching all the coupling capacitors in circuit and discretely varying the length of all the coupled-line sections synchronously. A selection (indexed as a–e in Fig. 6) of the 16 possible tuning states are shown in Fig. 9 along with the corresponding simulated responses. The filter gives almost constant fractional bandwidth across the complete tuning range, except for a slight reduction at low values of coupled-line length (from 14% to 11.5%). The variation in insertion loss across the tuning range is also minimal. This reflects a constant unloaded Q of the resonators regardless of tuning position.

TABLE III
DETAILS OF A NUMBER OF BANDWIDTH TUNING POINTS

Tuning point	Mathematically derived f_0 (MHz)	W (%)	n_{Li}	n_{Ci}	n_{Le}	n_{Ce}	Error	Measured f_0 (MHz)	W (%)
i	798	14.8	7	7	7	7	0.037	805	14.3
ii	826	13.0	7	6	7	6	0.426	835	13.5
iii	770	9.8	8	5	8	6	0.617	756	9.9
iv	820	8.0	7	4	8	5	0.453	857	9.2
v	755	6.9	8	4	9	5	0.285	760	8.8
vi	794	4.9	8	3	9	4	0.273	789	5.7
1	430	14.8	13	13	13	13	0.031	434	14.5
2	438	13.9	13	12	13	12	0.412	443	14.4
3	448	11.7	13	10	13	11	0.475	453	13.1
4	453	10.4	13	9	14	10	0.629	455	11.0
5	430	8.6	14	8	15	10	0.326	431	8.8
6	437	7.5	14	7	15	9	0.425	440	8.0
7	436	5.8	14	6	16	8	0.274	441	6.3
8	451	4.6	14	5	16	7	0.139	447	6.0
9	448	2.9	14	4	17	6	0.241	452	4.0
10	428	2.5	15	4	18	6	0.13	426	3.8

Key to abbreviations:
f_0 - centre-frequency
n_{Li}, n_{Ci}, n_{Le}, n_{Ce} – number of interior (i) or end (e) length segments (L) or coupling capacitors (C) required to achieve the desired centre-frequency and FBW.

B. Bandwidth Tuning

To test the bandwidth tuning capabilities of the filter, two groups of sample points were chosen, which had similar center frequencies, but a range of bandwidth values. The two groups are indexed in Fig. 6 clustered around 800 and 400 MHz. The details of these points are given in Table III. Each of the points corresponds to a local minimum in the error function. The center frequency and fractional bandwidth for each of the points were obtained from Fig. 6 and are based on empirical relationships extrapolated from a selection of values calculated using the synthesis process. The four central columns of the table are the numbers of coupling capacitors and length segments required to achieve each fractional bandwidth and center frequency. In most cases, these numbers have been rounded from a noninteger number, indicating that a perfect filter shape cannot be obtained. The corresponding error value reflects the extent of this rounding in each case.

Each of these points was measured using the experimental filter and the actual center frequencies and bandwidths are listed in the final columns of Table III. Since the mathematically derived values of center frequency and bandwidth are approximate, there is some variation in their correlation with the measured values. The measured results of the different tuning states are shown in Figs. 10–12. For clarity, the measured results for the 430-MHz cluster have been grouped around common center frequencies and split over two plots.

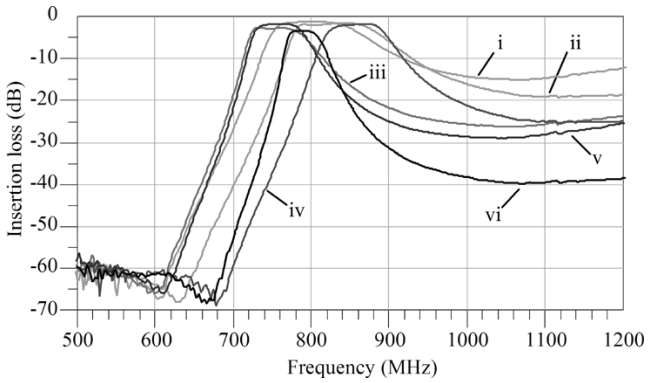

Fig. 10. Measured insertion loss of experimental lumped-distributed coupled-line filter for six bandwidth tuning points detailed in Table III.

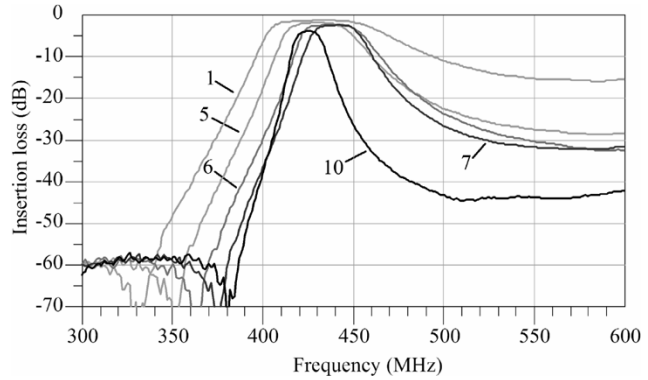

Fig. 11. Measured insertion loss of experimental lumped-distributed coupled-line filter for five of the ten bandwidth tuning points detailed in Table III.

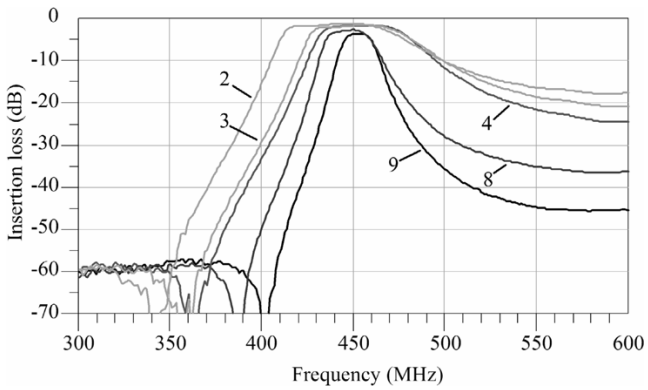

Fig. 12. Measured insertion loss of experimental lumped-distributed coupled-line filter for five of the ten bandwidth tuning points detailed in Table III.

C. Discussion

The results shown here demonstrate that both wide range center-frequency and bandwidth tuning are possible using the lumped-distributed coupled-line topology. The experimental filter could be tuned in discrete steps over two octaves of center frequency, i.e., 350 MHz–1.4 GHz, with little degradation in the response. In addition, a number of different bandwidth settings could be selected, ranging from 3.8% to 14.5%; a 3.8 : 1 tuning range. A disadvantage is that the tuning ranges are not uniform; at lower frequencies, there is a greater choice of both center frequency and bandwidth. However, it may be possible to provide more consistent tuning resolution through the use of reconfigurable resonators, which can be switched either in parallel or series [15].

An essential aspect of tunable filter design is the effect of the tuning mechanism on the filter insertion loss. Simulations using realistic values for the contact resistance (0.5 Ω) and Q (50) of the RF MEMS contact and capacitive switches show that the unloaded Q of the resonators varies from a nominal value of 28 by only 21% across both frequency and bandwidth tuning ranges. This indicates that the filter structure is relatively independent of the number of tuning elements employed.

VI. Conclusion

The lumped-distributed coupled-line filter topology described in this paper was developed to provide a filter structure, which could be tuned in both bandwidth and center frequency over a wide range. The shunt and parallel connections of the multiple distributed switching elements means that the losses remain constant regardless of the number of switching elements employed. The number and range of the tuning steps is thus only limited by the number of switching elements, not by losses in the filter structure itself. The antiphase relationship between the EM and capacitive coupling coefficients of lumped-distributed coupled lines allows for very low fractional bandwidths without the need for widely spaced lines. A filter synthesis procedure has been developed based on network models of the coupled lines, allowing the parameters of the filter to be derived from standard filter prototype values. This procedure and the performance of the lumped-distributed coupled-line filter have been verified through experimental results.

Further study will involve reducing the filter to a standard combline structure through the intelligent implementation of the filter and switching elements. This will lead to greatly improved harmonic performance and a twofold reduction in electrical size. The use of lower coupling capacitance values to improve the upper stopband rejection, as described in this paper, will result in a high-performance discretely tunable planar filter, reconfigurable in both center frequency and bandwidth.

Acknowledgment

Author B. E. Carey-Smith is grateful to C. J. Carpenter, University of Bristol, Bristol, U.K., for valuable discussions in the course of this study. The authors would like to acknowledge the contributions of their colleagues from Siemens AG, France Télécom—Research and Development, Centre Suisse d'Electronique et de Microtechnique S.A., King's College London, Motorola SA, Panasonic European Laboratories GmbH, Regulierungsbehörde für Telekommunikation und Post, Telefonica Investigacion Y Desarrollo S.A. Unipersonal, Toshiba Research Europe Ltd., TTI Norte S.L., University of Southampton, University of Portsmouth, Siemens ICN S.p.A., 3G.com Technologies Ltd., and Motorola Ltd.

REFERENCES

[1] J. R. Macleod, M. A. Beach, P. A. Warr, and T. Nesimoglu, "A software defined radio receiver test-bed," in *Proc. 54th Vehicular Technol. Conf.*, vol. 3, 2001, pp. 1565–1569.

[2] R. D. Streeter, C. A. Hall, R. Wood, and R. Mahadevan, "VHF high-power tunable RF bandpass filter using microelectromechanical (MEM) microrelays," *Int. J. RF Microwave Computer-Aided Eng.*, vol. 11, pp. 261–275, Sep. 2001.

[3] J. Brank, J. Yao, M. Eberly, A. Malczewski, K. Varian, and C. Goldsmith, "RF MEMS-based tunable filters," *Int. J. RF Microwave Computer-Aided Eng.*, vol. 11, pp. 276–284, Sep. 2001.

[4] R. L. Borwick, III, P. A. Stupar, J. F. DeNatale, R. Anderson, and R. Erlandson, "Variable MEMS capacitors implemented into RF filter systems," *IEEE Trans. Microw. Theory Tech.*, vol. 51, pp. 315–319, Jan. 2003.

[5] R. M. Young *et al.*, "Low-loss bandpass RF filter using MEMS capacitance switches to achieve a one-octave tuning range and independently variable bandwidth," in *IEEE MTT-S Int. Microwave Symp. Dig.*, Jun. 2003, pp. 1781–1784.

[6] J. R. Macleod, T. Nesimoglu, M. A. Beach, and P. A. Warr, "Miniature distributed filters for software re-configurable radio applications," in *Proc. Information Society Technologies Mobile Wireless Telecommunications Summit 2002*, Jun. 2002, pp. 159–163.

[7] Y. Liu, A. Borgioli, A. S. Nagra, and R. A. York, "Distributed MEMS transmission lines for tunable filter applications," *Int. J. RF Microwave Computer-Aided Eng.*, vol. 9, pp. 254–260, Jul. 1999.

[8] E. Fourn *et al.*, "Bandwidth and central frequency control on tunable bandpass filter by using MEMS cantilevers," in *IEEE MTT-S Int. Microwave Symp. Dig.*, Jun. 2003, pp. 523–526.

[9] C. Rauscher, "Reconfigurable bandpass filter with a three-to-one switchable passband width," *IEEE Trans. Microw. Theory Tech.*, vol. 51, pp. 573–577, Feb. 2003.

[10] B. Carey-Smith, P. A. Warr, M. A. Beach, and T. Nesimoglu, "Tunable lumped-distributed capacitively coupled transmission-line filter," *Electron. Lett.*, vol. 40, pp. 434–436, Apr. 2004.

[11] R. Mongia, I. J. Bahl, and P. Bhartia, *RF and Microwave Coupled-Line Circuits*. Norwood, MA: Artech House, 1999, pp. 150–151.

[12] J.-S. Hong and M. J. Lancaster, "Couplings of microstrip square open-loop resonators for cross-coupled planar microwave filters," *IEEE Trans. Microw. Theory Tech.*, vol. 44, pp. 2099–2109, Nov. 1996.

[13] G. L. Matthaei, L. Young, and E. M. Jones, *Microwave Filters, Impedance-Matching Networks and Coupling Structures*. Norwood, MA: Artech House, 1980, pp. 636–638.

[14] S. B. Cohn, "Direct-coupled-resonator filters," in *Proc. IRE*, vol. 45, Feb. 1957, pp. 187–196.

[15] B. Carey-Smith, P. A. Warr, M. A. Beach, and T. Nesimoglu, "A MEMS-ready wide tuning range planar resonator with application to microwave flexible filters," in *Proc. Asia–Pacific Microwave Conf.*, Nov. 2003, pp. 1581–1584.

Bruce E. Carey-Smith received the B.E. degree in electrical and electronic engineering from the University of Canterbury, Christchurch, New Zealand, in 1995, and is currently working toward the Ph.D. degree in electrical engineering at the University of Bristol, Bristol, U.K.

From 1995 to 2002, he was with Tait Electronics Ltd., Christchurch, New Zealand, where he was involved in the design of RF circuits and systems for mobile radio applications. He subsequently joined the University of Bristol, as a Research Associate with the Centre for Communications Research, where his current research interests are in the area of tunable microwave circuits for software reconfigurable radio.

Paul A. Warr received the B.Eng. degree in electronics and communications from The University of Bath, Bath, U.K., in 1994, and the M.Sc. degree in communications systems and signal processing and Ph.D. degree for his work on octave-band linear receiver amplifiers from The University of Bristol, Bristol, U.K., in 1996 and 2001, respectively.

He was with the Marconi Company, where he was involved with secure high-redundancy cross-platform communications. He is currently a Lecturer of radio frequency engineering with the University of Bristol, where his research concerns the front-end aspects of software (reconfigurable) radio and diversity-exploiting communication systems, responsive linear amplifiers, flexible filters, and linear frequency translation. His research has been supported by the U.K. Department of Trade and Industry (DTI)/Engineering and Physical Sciences Research Council (EPSRC) alongside Commission of the European Communities (CEC) Advanced Communications Technologies and Services (ACTS) and Information Society Technologies (IST) programs and industrial collaborators.

Dr. Warr is a member of the Executive Committee of the Institution of Electrical Engineers (IEE), U.K., Professional Network on Communication Networks and Services.

Mark A. Beach (A'90) received the Ph.D. degree from the University of Bristol, Bristol, U.K., in 1989.

In 1989, he joined the University of Bristol, as a member of academic staff. He is currently a Professor of radio systems engineering with the University of Bristol. He has made contributions to the European collaborative projects, TSUNAMI, SATURN, ROMANTIK, TRUST, and more recently, SCOUT. His current interests are focused on multiple-input–multiple-output (MIMO) channel characterization and the design and optimization of space-time coded wireless architectures for third-generation (3G) and fourth-generation (4G) wireless networks. His research interests include smart antenna technology for wireless, as well as analog RF circuitry for software definable radio (SDR).

Prof. Beach is a member of the Institution of Electrical Engineers (IEE), U.K., Professional Network on Antennas and Propagation. He is an editor for the IEEE TRANSACTIONS ON WIRELESS COMMUNICATIONS.

Tayfun Nesimoglu received the B.Sc. degree in electrical and electronic engineering from the Eastern Mediterranean University, Gazimağusa, Mersin, Turkey, in 1996, the M.Sc. degree in mobile, personal and satellite communications from the University of Westminster, Westminster, U.K., in 1997, and the Ph.D. degree in electrical engineering from the University of Bristol, Bristol, U.K., in 2002. His doctoral research concerned novel amplifier linearization techniques for broad-band mobile communication systems and software radio.

Since 2001, he has been a Research Associate with the University of Bristol, where he is involved in a number of European Union (EU) collaborative and industrial projects. His research interests include RF hardware, amplifier, mixer design and linearization, broad-band transmitter/receiver front-end architectures, and software radio enabling technologies. He has presented these research topics at international conferences. He has authored or coauthored numerous technical papers and has also reviewed several papers for IEEE conferences and journals.